Verification of a Many-Ion Simulator of the Dicke Model Through Slow Quenches across a Phase Transition

A. Safavi-Naini,[1,2] R. J. Lewis-Swan,[1,2] J. G. Bohnet,[3] M. Gärttner,[1,2,4] K. A. Gilmore,[3] J. E. Jordan,[3] J. Cohn,[5] J. K. Freericks,[5] A. M. Rey,[1,2] and J. J. Bollinger[3]

[1]*JILA, NIST and University of Colorado, 440 UCB, Boulder, Colorado 80309, USA*
[2]*Center for Theory of Quantum Matter, University of Colorado, Boulder, Colorado 80309, USA*
[3]*NIST, Boulder, Colorado 80305, USA*
[4]*Kirchhoff-Institut für Physik, Universität Heidelberg, Im Neuenheimer Feld 227, 69120 Heidelberg, Germany*
[5]*Department of Physics, Georgetown University, Washington, DC 20057, USA*

(Received 8 February 2018; revised manuscript received 26 June 2018; published 27 July 2018)

We use a self-assembled two-dimensional Coulomb crystal of ~70 ions in the presence of an external transverse field to engineer a simulator of the Dicke Hamiltonian, an iconic model in quantum optics which features a quantum phase transition between a superradiant (ferromagnetic) and a normal (paramagnetic) phase. We experimentally implement slow quenches across the quantum critical point and benchmark the dynamics and the performance of the simulator through extensive theory-experiment comparisons which show excellent agreement. The implementation of the Dicke model in fully controllable trapped ion arrays can open a path for the generation of highly entangled states useful for enhanced metrology and the observation of scrambling and quantum chaos in a many-body system.

DOI: 10.1103/PhysRevLett.121.040503

Introduction.—Quantum many-body systems featuring controllable coupled spin and bosonic degrees of freedom (d.o.f.) are becoming a powerful platform for the realization of quantum simulators with easily tunable parameters. These include, for example, cavity QED (CQED) systems [1–8] and trapped-ion arrays [9,10]. Most often, these systems have been operated in the far detuned regime where the bosons do not play an active role in the many-body dynamics and, instead, are used to mediate spin-spin coupling between particles. Great progress has been realized in this effective spin-model regime including the implementation of long range Ising models with and without an external transverse field and the exploration of rich physics with them such as entanglement dynamics [1,2,11–17], many-body localization [18], time crystals [19], and dynamical phase transitions [20,21]. On the other hand, excluding few particle implementations [22–30], the regime where the bosonic d.o.f. actively participate in the many-body dynamics has remained largely unexplored.

In this work, we focus on this regime and report the implementation of a simulator of the Dicke model, an iconic model in cavity QED which describes the coupling of a (large) spin and an oscillator, in a self-assembled two-dimensional (2D) crystal of ions. The Dicke model is of broad interest as it exhibits rich physics including quantum phase transitions and nonergodic behavior [31]. More recently, it has gained renewed attention due to the implementation of the closely related Tavis-Cummings model in circuit QED [32] and its realization in CQED experiments with cold bosonic atoms [6–8,33,34]. In the latter, the Dicke model emerged as an effective Hamiltonian when one encodes a two-level system in two different momentum states of a Bose-Einstein condensate (BEC) coupled by the cavity field. Within this framework, the normal to superradiant transition maps to a transition between a standard zero momentum BEC and a quantum phase with macroscopic occupation of the higher-order momentum mode and the cavity mode.

While CQED experiments have used the intracavity light intensity and time of flight images to monitor the phase transition, here, instead, we probe the two distinct quantum phases of the Dicke model by using various controlled ramping protocols of a transverse field across the critical point (see Fig. 1). We benchmark the dynamics by experimentally measuring full distribution functions of the spin d.o.f. and then comparing them with theoretical calculations. The spin observables also allow us to infer the development of spin-phonon correlations.

Our implementation of the Dicke model and corresponding observation of the phase transition in a trapped ion setup represents a complementary work with respect to the CQED platform and illustrates the power and universal nature of quantum simulation. It also opens a path for using the high level control and tunability of trapped ion experiments for the generation of highly entangled states suitable to quantum metrology in the near term future, and for the exploration of regimes currently intractable to theory.

Spin-boson system.—Our experimental system is comprised of a 2D single-plane array of laser-cooled $^9Be^+$ ions in a Penning trap. The internal states forming the spin-$1/2$

system are the valence electron spin states in the Be^+ ion ground state which, in the 4.46 T magnetic field, are split by 124 GHz [16,17,36,37]. The interplay of the Coulomb repulsion and the electromagnetic confining potentials supports a set of normal vibrational modes of the crystal [38], which we couple to the spin d.o.f. via a spin-dependent optical dipole force (ODF), generated by the interference of a pair of lasers with beat note frequency ω_R [36]. The frequency ω_R is detuned from the center-of-mass (c.m.) mode frequency, $\omega_{\mathrm{c.m.}}$, by $\delta \equiv \omega_R - \omega_{\mathrm{c.m.}}$ (Fig. 1). The detuning is chosen to predominantly excite the c.m. mode which uniformly couples all the ions in the crystal [16]. In the presence of an additional transverse field,

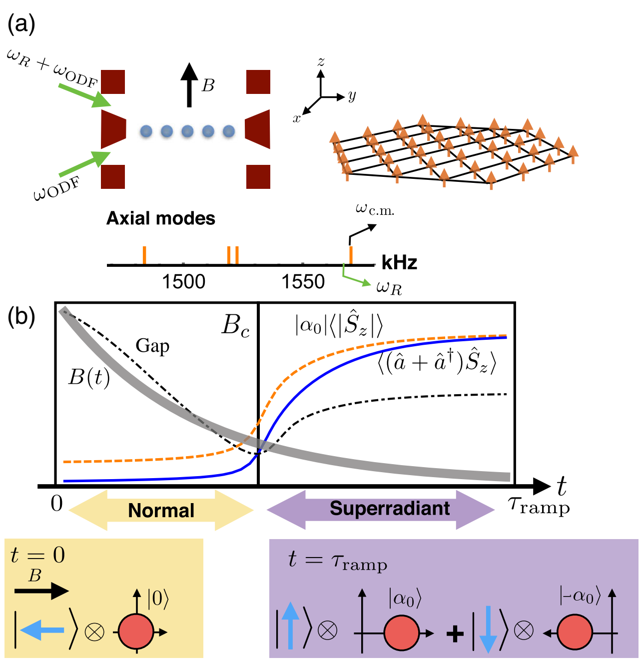

FIG. 1. Implementation and dynamical protocol. (a) The Dicke model is engineered with a Penning trap ion crystal of $N \sim 70$ ions by applying an optical dipole force, resonant only with the center of mass mode (which generates spin-phonon interactions) and resonant microwaves (which generate the transverse field). The system is initially prepared in the normal phase where all the spins point along the transverse field and are decoupled from the phonons. (b) As the transverse field is slowly turned off [using linear or exponential ramp (shown here) profiles with ramp time τ_{ramp}] the infinite system enters the superradiant phase after crossing the quantum critical point at $B(t_{\mathrm{crit}}) = B_c$ where the gap closes. The superradiant phase with macroscopic phonon population, ferromagnetically aligned spins and large spin-phonon entanglement is described by the order parameter $\langle(\hat{a}+\hat{a}^\dagger)\hat{S}_z\rangle$, which is tracked closely by the rescaled spin observable $|\alpha_0|\langle|\hat{S}_z|\rangle$. (c) In the perfectly adiabatic regime, the ground state evolves from a separable spin-paramagnetic and vacuum photon Fock state into a macroscopic spin-phonon cat state: a superposition of two opposite spin aligned and displaced-coherent phonon states (with the sign of the superposition dictated by a parity symmetry, see Supplemental Material [35]).

generated by resonant microwaves, we implement the Dicke Hamiltonian [39–41]

$$\hat{H}^{\mathrm{Dicke}}/\hbar = -\frac{g_0}{\sqrt{N}}(\hat{a}+\hat{a}^\dagger)\hat{S}_z + B(t)\hat{S}_x - \delta\hat{a}^\dagger\hat{a}. \quad (1)$$

in the frame rotating with ω_R. The operator $\hat{a}(\hat{a}^\dagger)$ is the bosonic annihilation (creation) operator for the c.m. mode, $B(t)$ is the time-varying strength of the applied transverse field, and g_0 represents the homogeneous coupling between each ion and the c.m. mode. Here, $\delta < 0$. We have introduced the collective spin operators $\hat{S}_\alpha = (1/2)\sum_j \hat{\sigma}_j^\alpha$ where $\hat{\sigma}_j^\alpha$ is the corresponding Pauli matrix for $\alpha = x, y, z$ which acts on the jth ion.

The Dicke Hamiltonian exhibits a quantum phase transition at $B_c = g_0^2/|\delta|$ in the thermodynamic limit, i.e., $N \to \infty$, [42–44], separating the normal ($B > B_c$) and superradiant ($B < B_c$) phases. The Hamiltonian remains unchanged under the simultaneous transformations $\hat{S}_x \to \hat{S}_x$, $\hat{S}_z \to -\hat{S}_z$, $\hat{S}_y \to -\hat{S}_y$, and $\hat{a} \to -\hat{a}$. These are generated by the parity operator $\hat{\Pi} = e^{i\pi[\hat{a}^\dagger\hat{a}+\hat{S}_x+(N/2)]}$.

In the strong-field regime of the normal phase, $B \gg B_c$, the spins and phonons decouple into a product state. When $|B| > |\delta|$ the corresponding ground state, $|\psi_{0,N/2}^{\mathrm{Nor}}\rangle$, and low lying excitations, $|\psi_{n=1,2,\ldots}^{\mathrm{Nor}}\rangle$, are $|\psi_{n,N/2}^{\mathrm{Nor}}\rangle = |n\rangle \otimes |-N/2\rangle_x$. We use $|n\rangle$ to denote Fock states and $|M\rangle_{\alpha=\{x,y,z\}}$ to denote the fully symmetric ($S = N/2$) eigenstates which satisfy $\hat{S}_\alpha|M\rangle_\alpha = M|M\rangle_\alpha$ with $-N/2 \le M \le N/2$.

In the weak-field limit, $B \ll B_c$, of the superradiant phase, the spin and phonon d.o.f. are entangled and the ground state becomes degenerate in the thermodynamic limit. For a finite system, it approaches $|\psi_{0,N/2}^S\rangle = (1/\sqrt{2})(|\alpha_0,0\rangle \otimes |N/2\rangle_z \pm |-\alpha_0,0\rangle \otimes |-N/2\rangle_z)$ as $B \to 0$, where we have introduced the displaced Fock states $|\alpha, n\rangle \equiv \hat{D}(\alpha)|n\rangle$ with $\hat{D}(\alpha) = e^{\alpha\hat{a}^\dagger - \alpha^*\hat{a}}$ the associated displacement operator [45]. Here, the sign of the superposition is dictated by the parity symmetry: for even N, the ground state will be the symmetric superposition with $\langle e^{i\pi[\hat{a}^\dagger\hat{a}+\hat{S}_x+(N/2)]}\rangle = 1$, while for odd N, the ground state is the antisymmetric superposition with $\langle e^{i\pi[\hat{a}^\dagger\hat{a}+\hat{S}_x+(N/2)]}\rangle = -1$. In this weak-field regime, the spins exhibit ferromagnetic order, characterized by the nonzero value of the order parameter $|\hat{S}_z|$, while the phonon mode acquires a macroscopic expectation value equal to $|\alpha_0|^2$, where $\alpha_0 = g_0\sqrt{N}/(2\delta)$. The low-lying excitations correspond to displaced Fock states, $|\psi_{n>0,N/2}^S\rangle$, if $\delta^2 < g_0^2$ and to spin-flips along $\hat{z}$, $|\psi_{0,M<N/2}^S\rangle$, if $\delta^2 > g_0^2$.

Slow quench dynamics.—At the start of the experimental sequence (see Fig. 1), we prepare the initial spin state $|-N/2\rangle_x$ with the aid of a resonant microwave pulse. Doppler-limited cooling of the phonon d.o.f. leads to an initial transverse phonon thermal state with mean

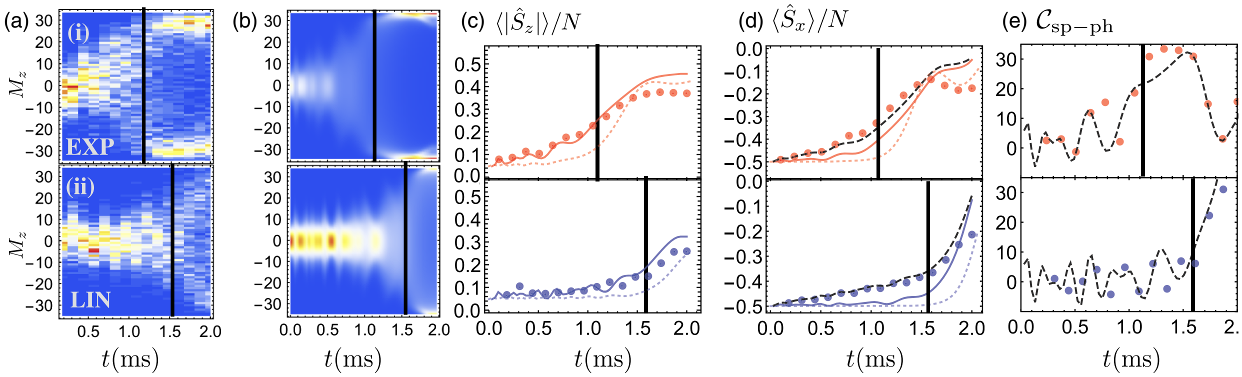

FIG. 2. Benchmarking the simulator: Column (a) shows the experimentally measured distribution function along z, and (b) the corresponding theoretical simulations neglecting decoherence. Column (c) shows the corresponding mean values of the magnetization $\langle|\hat{S}_z|\rangle$, (d) spin projection $\langle\hat{S}_x\rangle$, and (e) $\mathcal{C}_{\mathrm{sp-ph}} \equiv \langle(\hat{a}+\hat{a}^\dagger)\hat{S}_y\rangle$. The filled circles are experimental measurements (statistical error is on the order of marker size), the colored solid and black dashed lines are the theory results without and with dephasing [the latter curve is absent in panel (c) as the z magnetization is less sensitive to this dominant source of decoherence] and the colored dotted lines are the Lipkin model results. We indicate the time at which B_c is reached in each ramp by a vertical line. The initial field is $B(t=0)/(2\pi) \approx 7.1$ kHz, $g_0/(2\pi) \approx 1.32$ kHz, $\delta/(2\pi) = -1$ kHz, and $J/(2\pi) = 1.75$ kHz. Respective ion numbers are $N = 68$ [EXP—row (i)] and $N = 69$ [LIN—row (ii)].

occupation $\bar{n} \sim 6$. For these parameters, the system starts in the normal phase close to the ground state. The transverse field is then quenched to zero (while the spin-phonon coupling and detuning are held constant) according to two different profiles: (i) Linear (LIN): $B(t) = B_0(1 - t/\tau_{\mathrm{ramp}})$, and (ii) Exponential (EXP): $B(t) = B_0 e^{-t/\tau}$. We set $\tau_{\mathrm{ramp}} = 2$ ms and $\tau \approx 600$ μs.

To characterize the performance of the simulator and the entrance into the superradiant phase, we experimentally measure the full spin distribution along the z direction (Fig. 2) by determining the global ion fluorescence scattered from the Doppler cooling laser on the cycling transition for ions in $|\uparrow\rangle_z$ [16,17,36,37]. For repeated experimental trials, we infer the state populations, $N_\uparrow$ and $N_\downarrow$ and calculate the spin-projection $M_z \equiv N_\uparrow - N/2$ for each experimental shot by counting the total number of photons collected on a photomultiplier tube in a detection period, typically 5 ms. Off-resonant light scattering from the ODF lasers is our main source of decoherence dominated by single-particle dephasing at a rate Γ_{el} [46].

As noted above, the experimental implementation and corresponding numerical simulations were carried out with $N \approx 70$ atoms. However, a well-defined crossover between the normal and superradiant phases, signaled by a well-defined minimum in the energy gap between the ground and excited states of the same parity sector [see Fig. 1(b)], appears for crystals larger than $N \gtrsim 5$ (see Supplemental Material [35]).

Our theory-experiment comparisons are based on numerical solutions of the Dicke model dynamics combined with thermal averaging. If decoherence is neglected, the spin d.o.f. is constrained to the $S = N/2$ manifold. In this reduced Hilbert space, we can exactly treat the quantum dynamics. While for the non-negligible thermal phonon occupation in this experiment, a classical treatment of the dynamics is sufficient to reproduce the measured observables, a complete formulation of the quantum dynamics becomes necessary for colder conditions, when thermal fluctuations are insufficient to drive dynamics, and instead, quantum correlations must be properly accounted for. We observe good qualitative agreement between the experimental spin probability distribution and the theoretically computed unitary dynamics as shown in Figs. 2(a) and 2(b). In particular, both show a clear transition to a bimodal structure as the field strength is ramped down through B_c (indicated by the black vertical line in each plot), with some "smearing" due to the thermal occupation of the phonons.

To quantitatively determine the performance of the simulator, we plot the evolution of the effective order parameter $\langle|\hat{S}_z|\rangle/N$ (experimental values are extracted from the measured distribution) in Fig. 2(c), which clearly builds up as one crosses B_c. The transition is not abrupt, and instead, exhibits small amplitude oscillations, most clearly evident in the theoretical calculations, which reflect the active role of the phonons given our initial finite thermal phonon occupation. In particular, our numerical simulations show a dependence of the oscillation amplitude on the initial phonon occupation (see Supplemental Material [35]). However, the frequency of the phonon oscillations is difficult to determine and interpret, as it depends on the complex interplay between the magnitude of the initial phonon occupation and the changing transverse field. We contrast this behavior with the case when the phonons can be adiabatically eliminated and realize an effective spin Lipkin model (LM), $\hat{H}^{\mathrm{LM}}/\hbar = (J/N)\hat{S}_z^2 + B(t)\hat{S}_x$ where $J = g_0^2/\delta$. The Lipkin model dynamics features a sharper increase in magnetization after the critical point, and significant disagreement with the experimental observations.

To further benchmark the simulator, we carry out similar measurements of the spin distribution along the x direction, extracted by applying a global $\pi/2$ pulse before the fluorescence measurement. Figure 2(d) shows the mean-value of the spin projection $\langle \hat{S}_x \rangle$. We observe x depolarization as the system exits the normal phase. The Lipkin model dynamics also exhibits a sharper depolarization across B_c than the one seen in the experiment. In this case, however, we do observe deviations between the experiment and the ideal theory. The reason is that, unlike the z magnetization, this observable is strongly affected by dephasing. Since treating the full spin-boson system in the presence of decoherence is computationally challenging, we model the effect of dephasing as $\langle \hat{S}_x \rangle \to \langle \hat{S}_x \rangle e^{-\Gamma t}$ and $\langle \hat{S}_z \rangle \to \langle \hat{S}_z \rangle$ where $\Gamma = \Gamma_{\rm el}/2$, which is asymptotically valid in the $B \gg B_c$ and $B \ll B_c$ limits [47]. We can determine $\Gamma_{\rm el}$ experimentally when $B = 0$, and we find $\Gamma_{\rm el} \approx 120\ {\rm s}^{-1}$. However, at large B, most clearly evidenced in the LIN protocol, the demagnetization is faster than this estimate and is consistent with $\Gamma_{\rm el} = 280\,{\rm s}^{-1}$ [48]. For both ramps, we observe excellent agreement to the experiment when dephasing is accounted for.

Although measuring the phonon population might be possible following the protocol reported in Ref. [49], instead, we infer the buildup of spin-phonon correlations from the time evolution of the spin observable $\langle \hat{S}_x \rangle$. Specifically, we assume the dynamics of the system are captured by the Lindblad master equation for the density matrix of the spin-phonon system $\hat{\rho}$,

$$\frac{d\hat{\rho}}{dt} = -\frac{i}{\hbar}[\hat{H}^{\rm Dicke}, \hat{\rho}] + \frac{\Gamma_{\rm el}}{2}\sum_{i=1}^{N}(\hat{\sigma}_i^z \hat{\rho} \hat{\sigma}_i^z - \hat{\rho}), \qquad (2)$$

where single-particle dephasing is taken to be the dominant decoherence mechanism. From the master equation, we derive the equation of motion $(d/dt)\langle \hat{S}_x \rangle$, and rearrange to obtain the relation (see Supplemental Material [35])

$$\mathcal{C}_{\rm sp-ph} \equiv \langle (\hat{a} + \hat{a}^\dagger)\hat{S}_y \rangle \equiv \frac{\sqrt{N}}{g_0}\left(\Gamma_{\rm el}\langle \hat{S}_x \rangle + \frac{d}{dt}\langle \hat{S}_x \rangle\right). \qquad (3)$$

We extract the spin-phonon correlation from the experimental data by evaluating the rhs of the above expression, and calculating the time-derivative numerically with a one-sided derivative. The results are plotted in Fig. 2(e). We use the same value of $\Gamma_{\rm el}$ as in Fig. 2(d). The results are compared with a theoretical calculation of $C_{\rm sp-ph}$ [again modeling dephasing using $\langle \hat{S}_x \rangle_\Gamma \equiv \langle \hat{S}_x \rangle_{\Gamma=0} e^{-\Gamma t}$]. In principle, the correlator vanishes when evaluated for the ground state at any field strength. However, for these slow quenches, it acquires a finite value, which, in particular, grows in the superradiant phase due to population of excited states. This is attributable due to diabatic excitations created during the ramping protocol or the initial thermal phonon ensemble. Thus, while the correlation $\mathcal{C}_{\rm sp-ph}$ shows similar dynamical features observed in the other observables, it gives an alternative insight into the excitations created during the ramp.

While we have used the two ramp profiles to benchmark the experiment, we note that the EXP ramp has more utility in preparing a final state close to the expected ground state $|\psi^S_{0,N/2}\rangle$ in the superradiant phase. For instance, the EXP ramp produces a clearer bimodal structure in the spin probability distribution along z, and the associated larger mean absolute spin projection $\langle |\hat{S}_z| \rangle$. Future experiments could improve assessment of the adiabaticity of the quench protocols by measuring any coherences present between the different spin components, as discussed below.

Accounting for spin-phonon entanglement will be key to properly diagnosing the generated many-body quantum state. For example, tracing out the phonons from $|\psi^S_{0,N/2}\rangle$ will exponentially suppress the coherence between the spin states $|\pm N/2\rangle_z$ (see Supplemental Material [35]). To benchmark the performance of the adiabatic dynamics, it is then highly desirable to, first, perform a protocol to disentangle the spins and phonons and, only after that, characterize the state by independently measuring the spins and the phonons without information loss.

To disentangle spin and phonons, we propose to instantaneously quench the detuning $\delta \to \delta' = 2\delta$ at the end of the ramp ($B \to 0$) and, then, let the system evolve for a time $t_d = \pi/\delta'$. At t_d, the phonons are coherently displaced by $-g_0\sqrt{N}/(2|\delta|)\langle S_z \rangle$ back to the origin, while the spins only acquire an irrelevant global phase [41]. The resulting disentangled state ideally becomes $(1/\sqrt{2})[|+\alpha_0,0\rangle|+N/2\rangle_z + |-\alpha_0,0\rangle|-N/2\rangle_z] \to (1/\sqrt{2})|0\rangle \otimes [|+N/2\rangle_z + |-N/2\rangle_z]$ which has maximal spin coherence.

Summary and discussion.—We have reported the experimental realization of a simulator of the Dicke model with a 2D ion crystal of ~70 ions and verified its dynamics through extensive theory-experiment comparisons. Our trapped-ion simulator provides a complementary approach to related realizations in cold atoms [6–8], which is a key step in benchmarking quantum simulators which go beyond the capacity of classical computation. Our realization of a many-ion simulator of the Dicke model also paves the way for future investigation of dynamical phase transitions [20,21], quantum chaos, and fast scrambling via out-of-time order correlation measurements [17,50–53]. Moreover, the tunability of the trapped-ion setup opens the possibility of investigating more general spin-boson models [54], in particular, by operating beyond the uniform coupling regime or the preparation of states outside the fully symmetric Dicke manifold.

The slow quench protocols demonstrated above present a path to generate highly entangled states useful for quantum enhanced metrology [55,56]. Cat states are a useful metrological resource as they are composed of a coherent superposition of states that are macroscopically displaced in phase space, leading to quantum-enhanced phase sensitivity up to the Heisenberg limit [57,58]. In particular, the spin-boson cat state $|\psi^S_{0,N/2}\rangle$ would be a metrological resource for sensing collective spin rotations [57], motional rotation [24,59], and coherent displacements for force sensing applications [60]. This could be achieved by using smaller systems (e.g., $N \sim 20$), reducing the initial thermal population of the phonon mode, and shifting the detuning δ away from B_c, which increases the minimum energy gap at the critical point, and consequently, the characteristic timescale to remain adiabatic (see Supplemental Material [35]). We expect this regime will be accessible in the near term future in part due to the successful implementation of electromagnetic induced transparency cooling [61].

The authors acknowledge fruitful discussions with J. Marino, M. Holland, and K. Lehnert. A. M. R. acknowledges support from the Defense Advanced Research Projects Agency (DARPA) and the Army Research Office Grant No. W911NF-16-1-0576, NSF Grant No. PHY1521080, JILA-NSF Grant No. PFC-173400, and the Air Force Office of Scientific Research and its Multidisciplinary University Research Initiative Grant No. FA9550-13-1-0086. M. G. acknowledges support from the DFG Collaborative Research Center Grant No. SFB1225 (ISOQUANT). J. E. J. also acknowledges support from the Leopoldina Research Fellowship, German National Academy of Sciences Grant No. LPDS 2016-15. J. K. F. and J. C. acknowledge support from NSF Grant No. PHYS-1620555. In addition, J. K. F. acknowledges support from the McDevitt bequest at Georgetown. Financial support from NIST is also acknowledged.

A. S.-N. and R. J. L.-S. contributed equally to this research.

[1] I. D. Leroux, M. H. Schleier-Smith, and V. Vuletić, Phys. Rev. Lett. **104**, 073602 (2010).
[2] O. Hosten, R. Krishnakumar, N. J. Engelsen, and M. A. Kasevich, Science **352**, 1552 (2016).
[3] H. Ritsch, P. Domokos, F. Brennecke, and T. Esslinger, Rev. Mod. Phys. **85**, 553 (2013).
[4] K. Baumann, C. Guerlin, F. Brennecke, and T. Esslinger, Nature (London) **464**, 1301 (2010).
[5] F. Brennecke, T. Donner, S. Ritter, T. Bourdel, M. Köhl, and T. Esslinger, Nature (London) **450**, 268 (2007).
[6] K. Baumann, C. Guerlin, F. Brennecke, and T. Esslinger, Nature (London) **464**, 1301 (2010).
[7] K. Baumann, R. Mottl, F. Brennecke, and T. Esslinger, Phys. Rev. Lett. **107**, 140402 (2011).
[8] J. Klinder, H. Keler, M. Wolke, L. Mathey, and A. Hemmerich, Proc. Natl. Acad. Sci. U.S.A. **112**, 3290 (2015).
[9] D. Porras and J. I. Cirac, Phys. Rev. Lett. **92**, 207901 (2004).
[10] K. Kim, M.-S. Chang, R. Islam, S. Korenblit, L.-M. Duan, and C. Monroe, Phys. Rev. Lett. **103**, 120502 (2009).
[11] R. Blatt and C. F. Roos, Nat. Phys. **8**, 277 (2012).
[12] P. Jurcevic, B. P. Lanyon, P. Hauke, C. Hempel, P. Zoller, R. Blatt, and C. F. Roos, Nature (London) **511**, 202 (2014).
[13] C. Senko, P. Richerme, J. Smith, A. Lee, I. Cohen, A. Retzker, and C. Monroe, Phys. Rev. X **5**, 021026 (2015).
[14] P. Richerme, Z.-X. Gong, A. Lee, C. Senko, J. Smith, M. Foss-Feig, S. Michalakis, A. V. Gorshkov, and C. Monroe, Nature (London) **511**, 198 (2014).
[15] R. Islam, E. E. Edwards, K. Kim, S. Korenblit, C. Noh, H. Carmichael, G.-D. Lin, L.-M. Duan, C.-C. J. Wang, J. K. Freericks, and C. Monroe, Nat. Commun. **2**, 377 (2011).
[16] J. G. Bohnet, B. C. Sawyer, J. W. Britton, M. L. Wall, A. M. Rey, M. Foss-Feig, and J. J. Bollinger, Science **352**, 1297 (2016).
[17] M. Gärttner, J. G. Bohnet, A. Safavi-Naini, M. L. Wall, J. J. Bollinger, and A. M. Rey, Nat. Phys. **13**, 781 (2017).
[18] J. Smith, A. Lee, P. Richerme, B. Neyenhuis, P. W. Hess, P. Hauke, M. Heyl, D. A. Huse, and C. Monroe, Nat. Phys. **12**, 907 (2016).
[19] J. Zhang, P. W. Hess, A. Kyprianidis, P. Becker, A. Lee, J. Smith, G. Pagano, I. D. Potirniche, A. C. Potter, A. Vishwanath, N. Y. Yao, and C. Monroe, Nature (London) **543**, 217 (2017).
[20] P. Jurcevic, H. Shen, P. Hauke, C. Maier, T. Brydges, C. Hempel, B. P. Lanyon, M. Heyl, R. Blatt, and C. F. Roos, Phys. Rev. Lett. **119**, 080501 (2017).
[21] J. Zhang, G. Pagano, P. W. Hess, A. Kyprianidis, P. Becker, H. Kaplan, A. V. Gorshkov, Z.-X. Gong, and C. Monroe, Nature (London) **551**, 601 (2017).
[22] J. S. Pedernales, I. Lizuain, S. Felicetti, G. Romero, L. Lamata, and E. Solano, Sci. Rep. **5**, 15472 (2015).
[23] D. Lv, S. An, Z. Liu, J.-N. Zhang, J. S. Pedernales, L. Lamata, E. Solano, and K. Kim, Phys. Rev. X **8**, 021027 (2018).
[24] K. G. Johnson, J. D. Wong-Campos, B. Neyenhuis, J. Mizrahi, and C. Monroe, Nat. Commun. **8**, 697 (2017).
[25] D. Kienzler, C. Flühmann, V. Negnevitsky, H.-Y. Lo, M. Marinelli, D. Nadlinger, and J. P. Home, Phys. Rev. Lett. **116**, 140402 (2016).
[26] C. Monroe, D. M. Meekhof, B. E. King, and D. J. Wineland, Science **272**, 1131 (1996).
[27] K. Toyoda, R. Hiji, A. Noguchi, and S. Urabe, Nature (London) **527**, 74 (2015).
[28] S. Debnath, N. M. Linke, S.-T. Wang, C. Figgatt, K. A. Landsman, L.-M. Duan, and C. Monroe, Phys. Rev. Lett. **120**, 073001 (2018).
[29] J. M. Raimond, M. Brune, and S. Haroche, Rev. Mod. Phys. **73**, 565 (2001).
[30] I. Aedo and L. Lamata, Phys. Rev. A **97**, 042317 (2018).
[31] A. Altland and F. Haake, Phys. Rev. Lett. **108**, 073601 (2012).
[32] J. M. Fink, R. Bianchetti, M. Baur, M. Göppl, L. Steffen, S. Filipp, P. J. Leek, A. Blais, and A. Wallraff, Phys. Rev. Lett. **103**, 083601 (2009).
[33] Z. Zhiqiang, C. Hui Lee, R. Kumar, K. J. Arnold, S. J. Masson, A. S. Parkins, and M. D. Barrett, Optica **4**, 424 (2017).

[34] Z. Zhiqiang, C. Hui Lee, R. Kumar, K. J. Arnold, S. J. Masson, A. L. Grimsmo, A. S. Parkins, and M. D. Barrett, Phys. Rev. A **97**, 043858 (2018).

[35] See Supplemental Material at http://link.aps.org/supplemental/10.1103/PhysRevLett.121.040503 for details of calculation and experiment.

[36] B. C. Sawyer, J. W. Britton, A. C. Keith, C.-C. Joseph Wang, J. K. Freericks, H. Uys, M. J. Biercuk, and J. J. Bollinger, Phys. Rev. Lett. **108**, 213003 (2012).

[37] M. J. Biercuk, H. Uys, A. P. Vandevender, N. Shiga, W. M. Itano, and J. J. Bollinger, Quantum Inf. Comput. **9**, 920 (2009).

[38] C.-C. Joseph Wang, A. C. Keith, and J. K. Freericks, Phys. Rev. A **87**, 013422 (2013).

[39] R. H. Dicke, Phys. Rev. **93**, 99 (1954).

[40] B. M. Garraway, Phil. Trans. R. Soc. A **369**, 1137 (2011).

[41] M. L. Wall, A. Safavi-Naini, and A. M. Rey, Phys. Rev. A **95**, 013602 (2017).

[42] C. Emary and T. Brandes, Phys. Rev. Lett. **90**, 044101 (2003).

[43] C. Emary and T. Brandes, Phys. Rev. E **67**, 066203 (2003).

[44] P. A. Ivanov and D. Porras, Phys. Rev. A **88**, 023803 (2013).

[45] A. Wunsche, Quantum Opt. **3**, 359 (1991).

[46] H. Uys, M. J. Biercuk, A. P. VanDevender, C. Ospelkaus, D. Meiser, R. Ozeri, and J. J. Bollinger, Phys. Rev. Lett. **105**, 200401 (2010).

[47] S. F. Huelga, C. Macchiavello, T. Pellizzari, A. K. Ekert, M. B. Plenio, and J. I. Cirac, Phys. Rev. Lett. **79**, 3865 (1997).

[48] This dephasing could be a result of the experimental system going beyond the Lamb-Dicke regime, which is implicitly assumed in the derivation of the Dicke Hamiltonian, Eq. (1).

[49] K. A. Gilmore, J. G. Bohnet, B. C. Sawyer, J. W. Britton, and J. J. Bollinger, Phys. Rev. Lett. **118**, 263602 (2017).

[50] S. H. Shenker and D. Stanford, J. High Energy Phys. 03 (2014) 67.

[51] A. Kitaev, in *Proceedings of the Fundamental Physics Prize Symposium*, 2014 (unpublished).

[52] J. Maldacena, S. H. Shenker, and D. Stanford, J. High Energy Phys. 08 (2016) 106.

[53] B. Swingle, G. Bentsen, M. Schleier-Smith, and P. Hayden, Phys. Rev. A **94**, 040302 (2016).

[54] A. Shankar, J. Cooper, J. G. Bohnet, J. J. Bollinger, and M. Holland, Phys. Rev. A **95**, 033423 (2017).

[55] P. Feldmann, M. Gessner, M. Gabbrielli, C. Klempt, L. Santos, L. Pezzè, and A. Smerzi, Phys. Rev. A **97**, 032339 (2018).

[56] J. Cohn, A. Safavi-Naini, R. J. Lewis-Swan, J. G. Bohnet, M. Garttner, K. A. Gilmore, E. Jordan, J. J. Bollinger, A. M. Rey, and J. K. Freericks, New J. Phys. **20**, 055013 (2018).

[57] J. J. Bollinger, W. M. Itano, D. J. Wineland, and D. J. Heinzen, Phys. Rev. A **54**, R4649 (1996).

[58] F. Toscano, D. A. R. Dalvit, L. Davidovich, and W. H. Zurek, Phys. Rev. A **73**, 023803 (2006).

[59] W. C. Campbell and P. Hamilton, J. Phys. B **50**, 064002 (2017).

[60] M. Penasa, S. Gerlich, T. Rybarczyk, V. Métillon, M. Brune, J. M. Raimond, S. Haroche, L. Davidovich, and I. Dotsenko, Phys. Rev. A **94**, 022313 (2016).

[61] A. Safavi-Naini, R. J. Lewis-Swan, J. G. Bohnet, M. Garttner, K. A. Gilmore, E. Jordan, J. Cohn, J. K. Freericks, A. M. Rey, and J. J. Bollinger (to be published).